

Earthquake Prediction: a Physical Basis

Scholz, Sykes and Aggarwal, 1973

Science

Objective

- Show that observed “unrelated” premonitory phenomena, to the date, have a common physical basis.

Evidences of precursory effects

- Crustal Surface uplift and tilt
- Variation of fluid pressure
- Variation of the electrical and magnetic field
- Radon emissions
- Increment between the ratio between number of small and large shocks
- Increase of the small earthquake activity
- Variation of V_p/V_s ratio

Evidences of precursory effects

- Laboratory experiences on rock samples also shows premonitory effects before failure:
 - Crack formation
 - Fluid diffusion
- Characteristic time of the premonitory effects is proportional to the earthquake magnitude

Dilatancy Phenomena

- Rocks samples undergoes an inelastic volumetric increase prior to the failure
- Is generated by formation and propagation of cracks.
- Start at stresses lower at the half of the breaking stress
- In saturated samples, the dilatancy undersaturate the rock

Dilatancy Phenomena

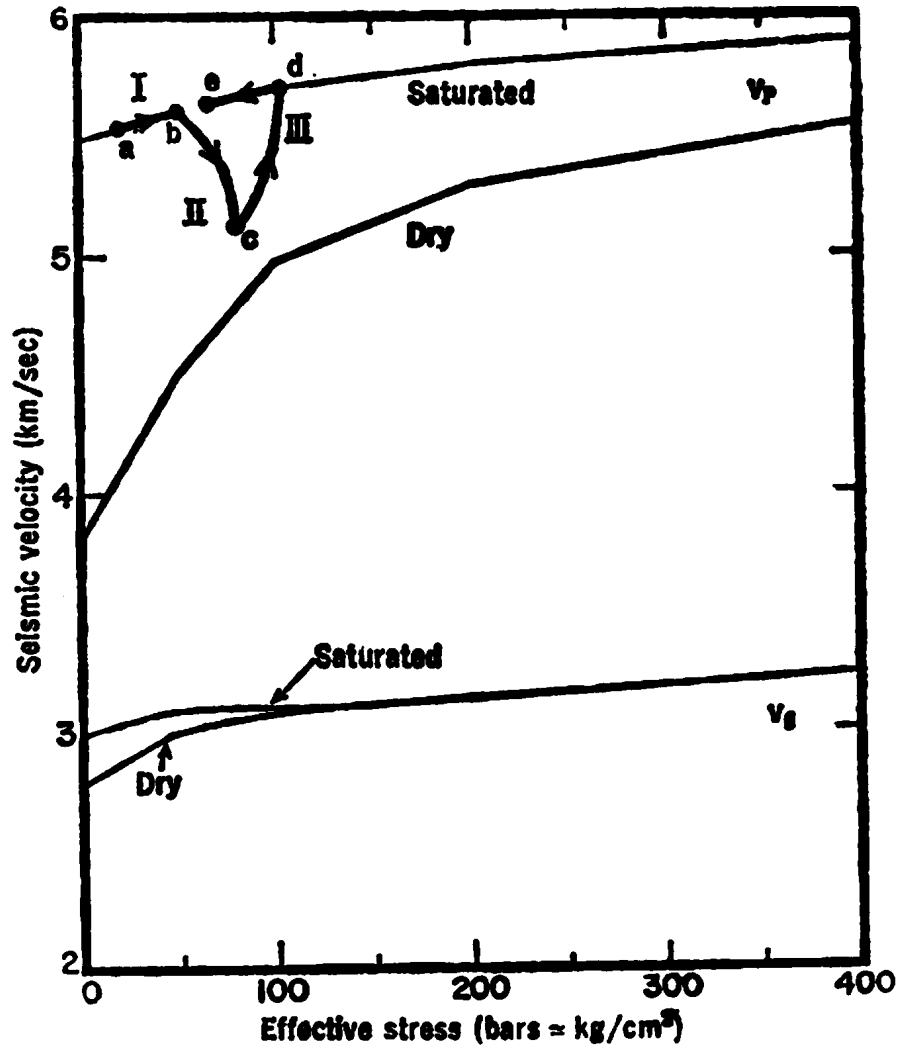
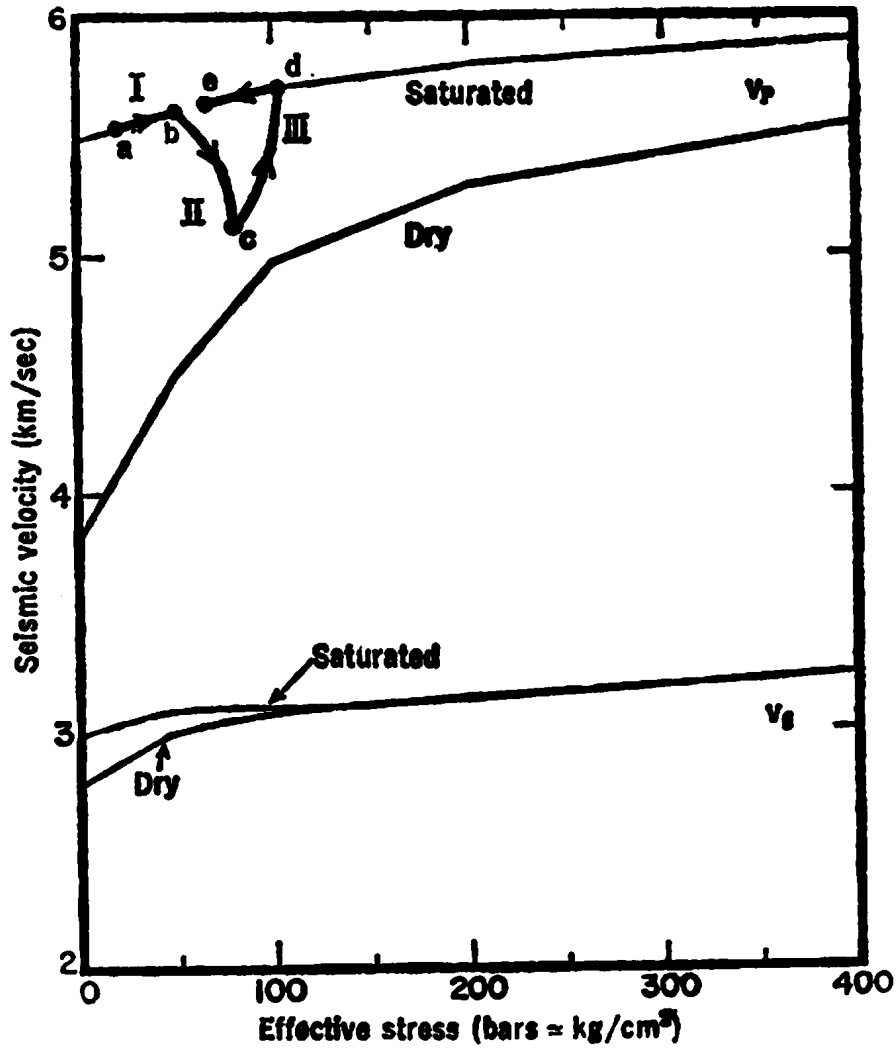


Fig. 1. Seismic velocities v_p and v_s as a function of the effective confining pressure for wet and dry Westerly granite (6). The P wave velocity follows along the direction of the arrows as dilatancy occurs in the earthquake source region (see text).

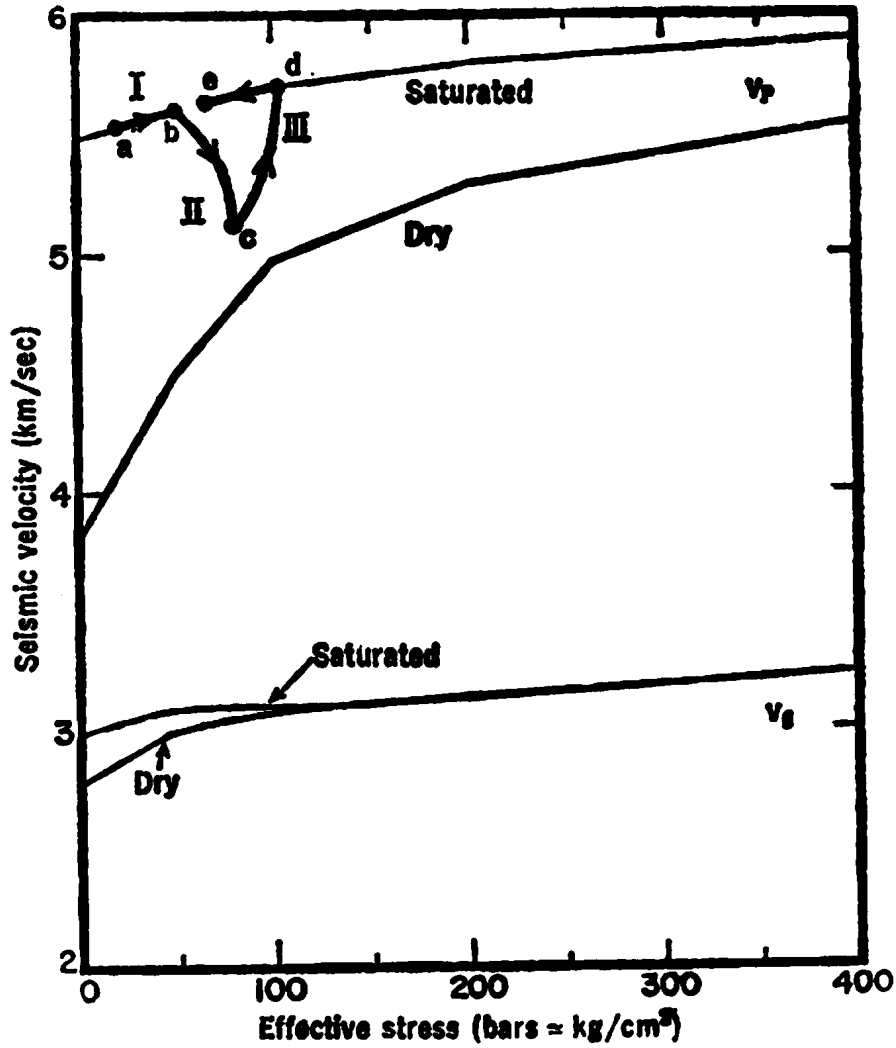
Dilatancy Phenomena



Dilatancy process in 3 Stages:

- Accumulation of tectonic strain
 - Slow process

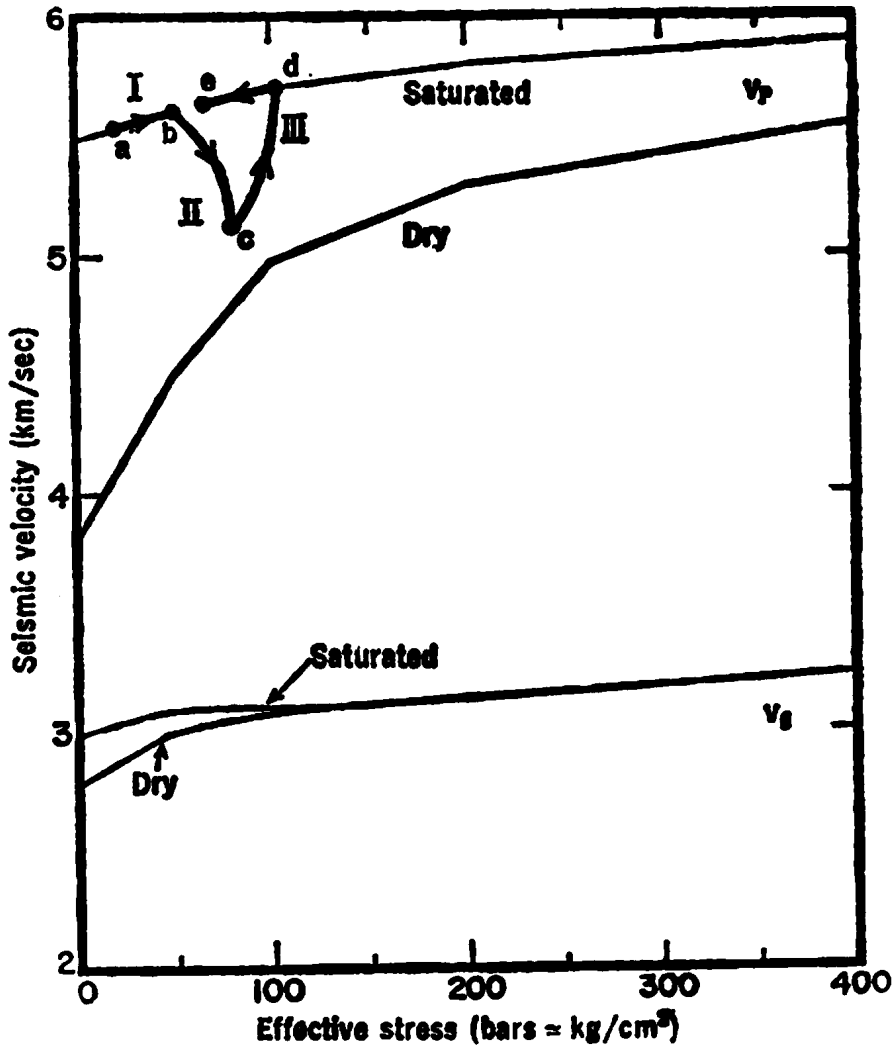
Dilatancy Phenomena



Dilatancy process in 3 Stages:

- Accumulation of tectonic strain
 - Slow process
- Beginning of the dilatancy faster the water flows
 - Undersaturation of the rock
 - Increase of the effective stress
 - V_p decrease (saturated rocks)
 - Dilatancy strengthening

Dilatancy Phenomena

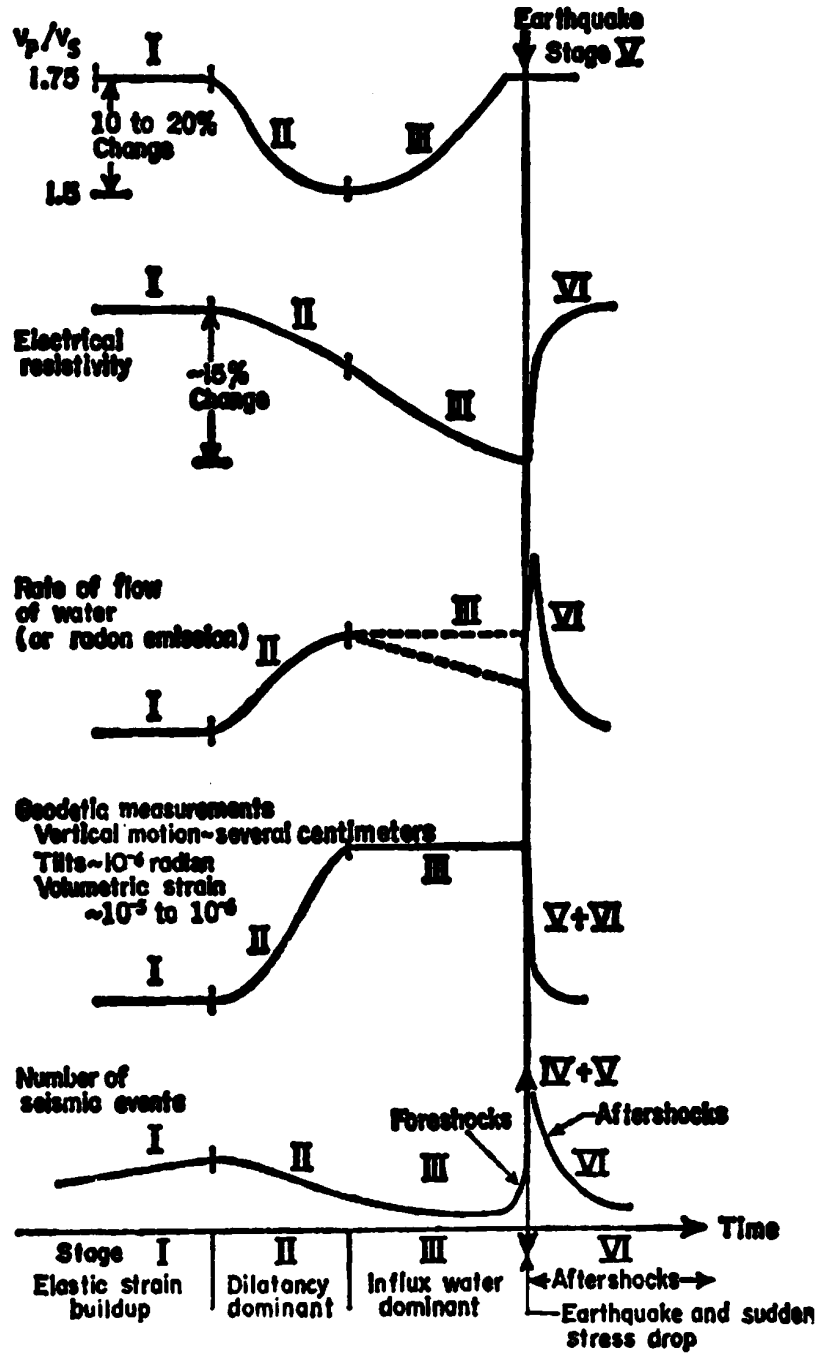


Dilatancy process in 3 Stages:

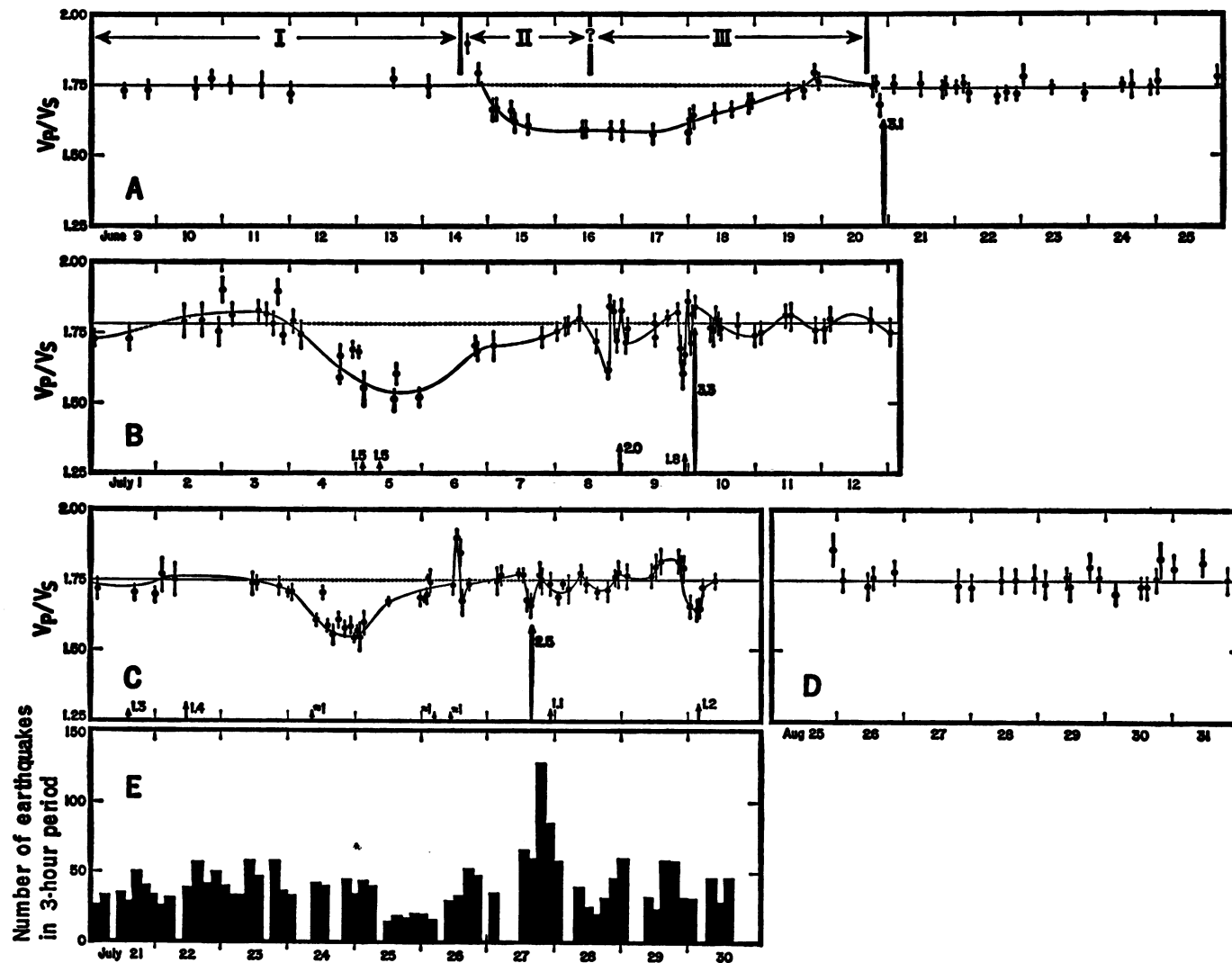
- Accumulation of tectonic strain
 - Slow process
- Beginning of the dilatancy faster the water flows
 - Undersaturation of the rock
 - Increase of the effective stress
 - v_p decrease (saturated rocks)
 - Dilatancy strengthening
- Water flows dominate the dilatancy
 - Re-saturation of the rock
 - v_p Increase
 - Pore pressure increase
 - Faulting triggering

Implications of the Dilatancy model

Fig. 3. Predicted changes in various physical parameters as a function of time during the earthquake cycle for the dilatancy model. Roman numerals indicate various stages in the cycle. Short-term fluctuations (stage IV), which are observed before some large earthquakes, are not indicated on the sketches. Note the striking correspondence between predicted premonitory effects and those observed (Figs. 4 to 7). The rate of water flow in stage III may vary as indicated by the dotted lines (see text). Radon emission may be a function not only of the rate of water flow but also of the rate of creation of new surface area by the growth of cracks.



1971 Blue Mountain Lake Earthquake Swarm, New York



1967 to 1969 Garm, U.S.S.R

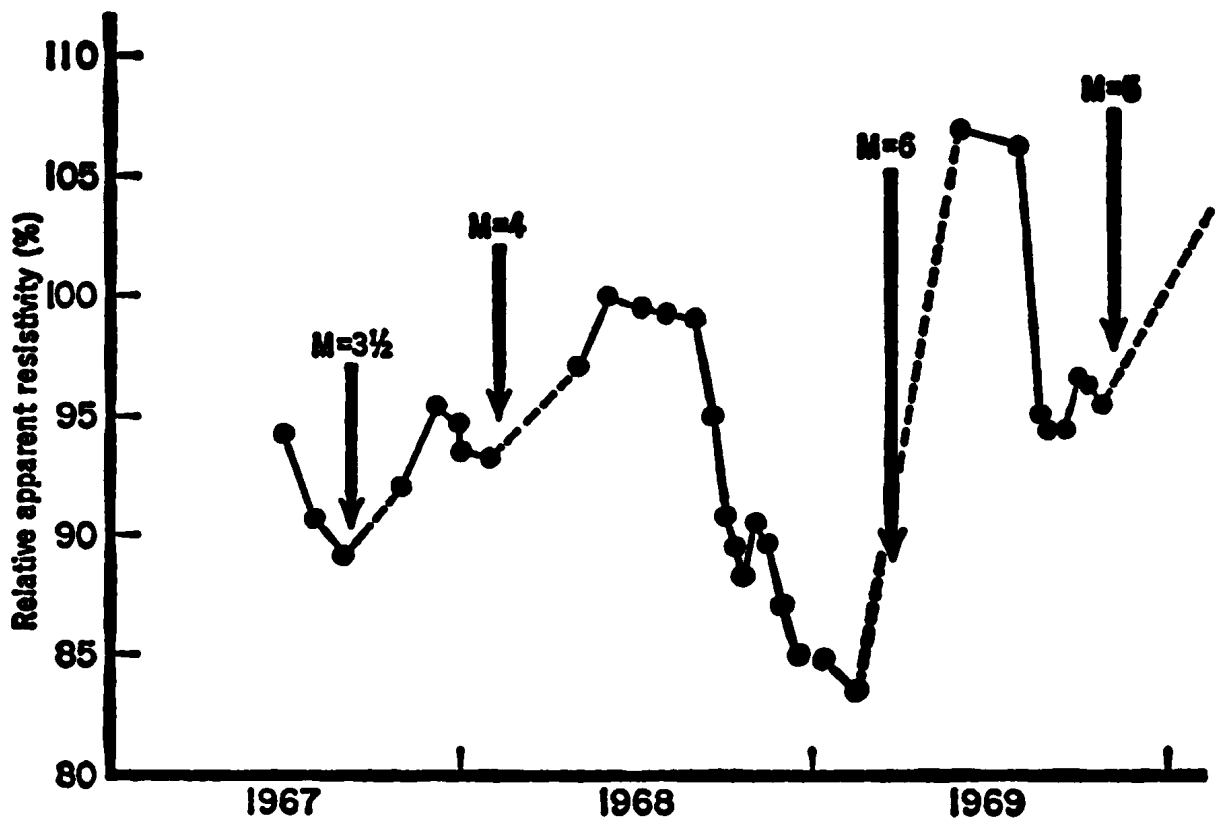


Fig. 5. Electrical resistivity anomalies observed before earthquakes at Garm, U.S.S.R. Note the marked drop in resistivity in the half-year period before the earthquake of $M = 6$ and the subsequent increase during and after the earthquake (10).

1964 Niigata Earthquake M 7.5, Japan

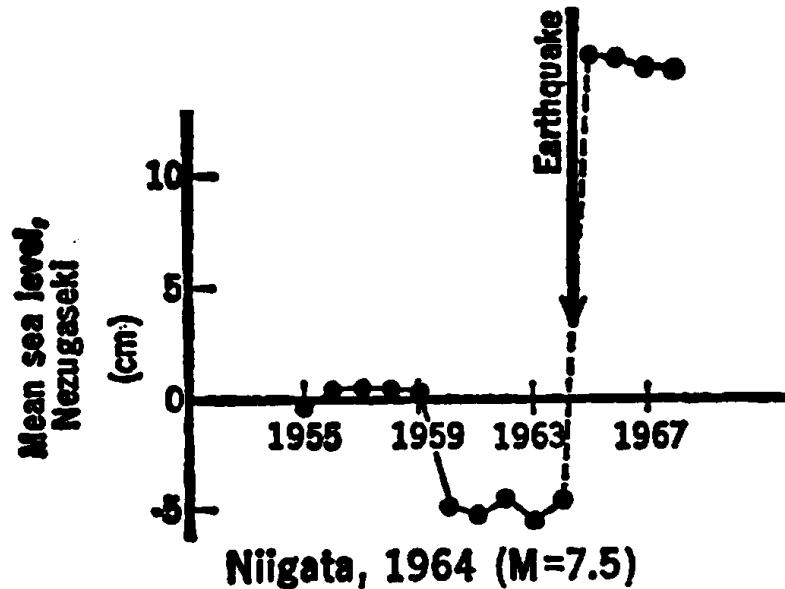
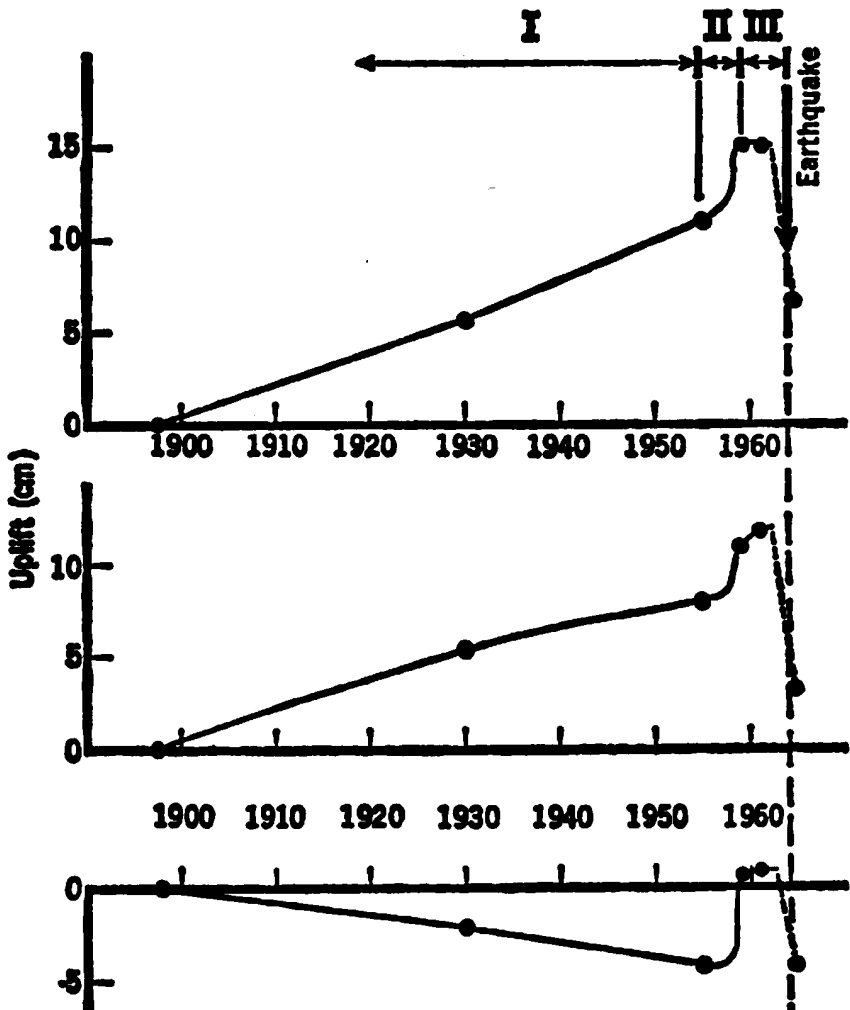


Fig. 4. The top three curves are elevation differences for three selected bench marks along a leveling route resurveyed several times before the 1964 earthquake at Niigata, Japan. The bottom curve presents mean sea level data from a tide gauge at Nezugaseki, near Niigata (a drop in sea level indicates uplift of the land). The recognizable stages in the earthquake cycle are indicated by Roman numerals. Note that premonitory effects are evident 6 years before this earthquake, $M = 7.5$. Data from (13).

1970 large aftershock of Fairsbank Earthquake, Alaska

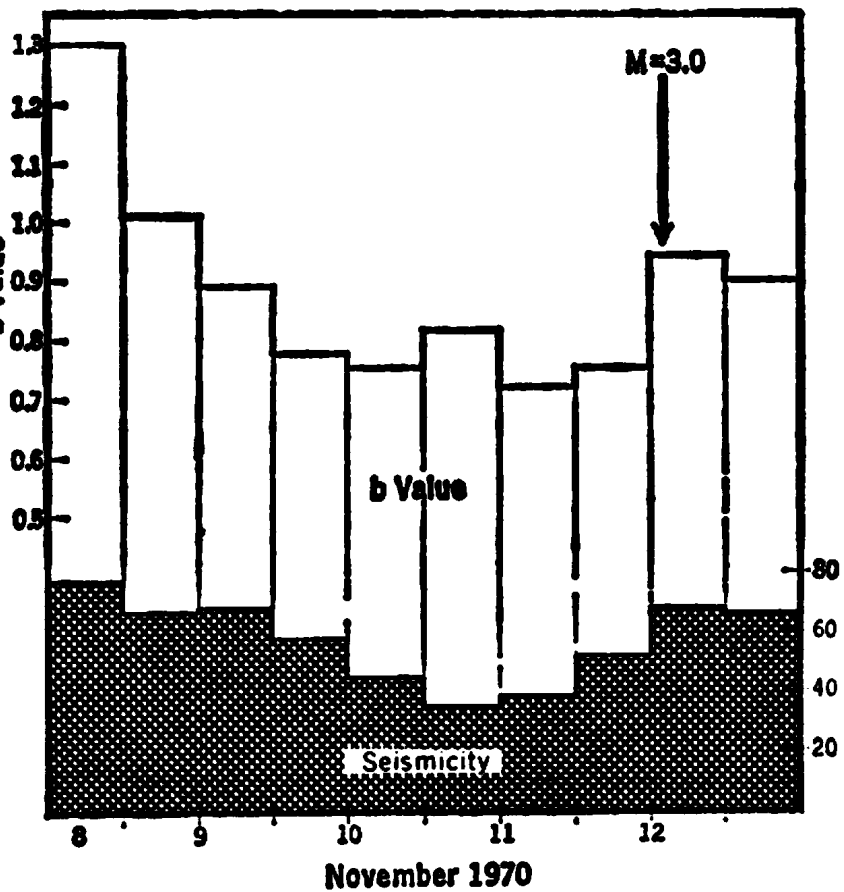


Fig. 7 (left). Observation of a drop in *b* value (top histogram) and seismicity rate (bottom histogram) for one of the larger aftershocks of the 1970 earthquake at Fairbanks, Alaska. Data from (19).

1966 Tashkent earthquake M 5.3,

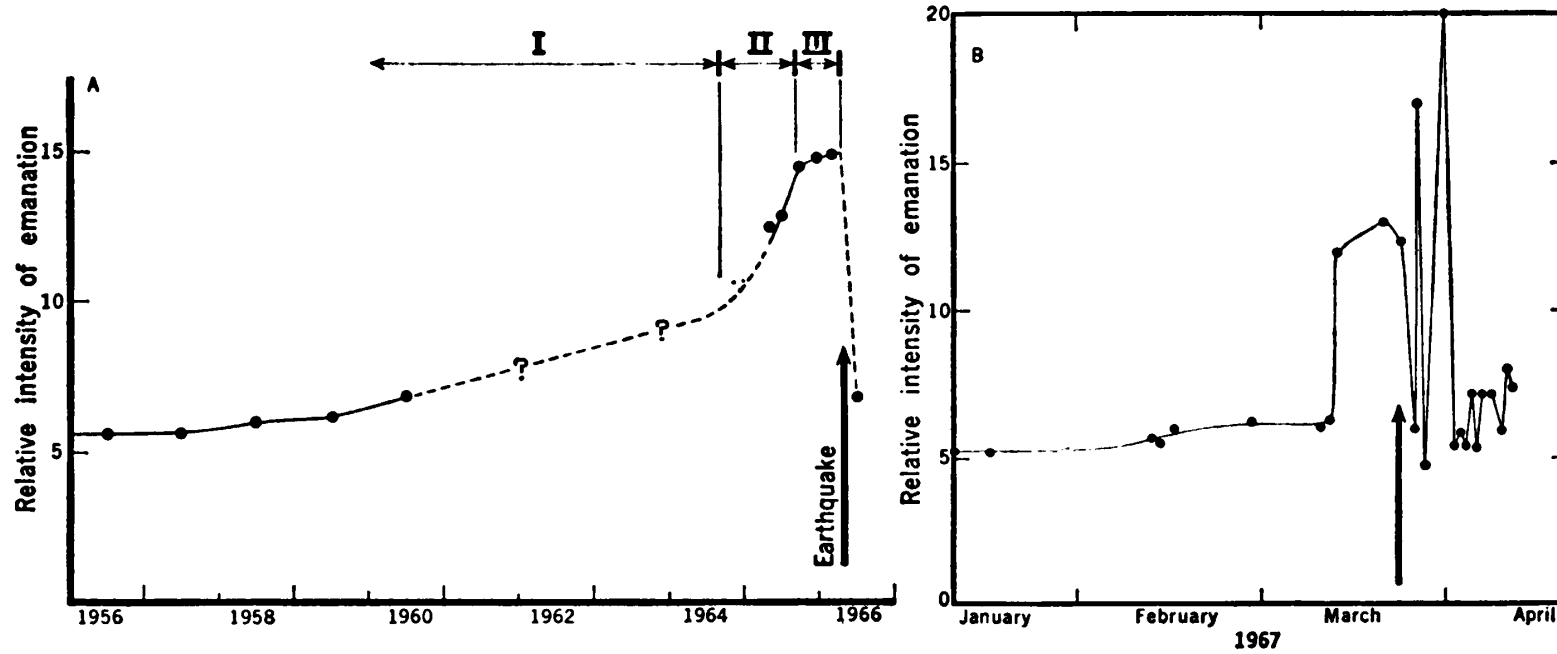


Fig. 6. Radon emission counts (17) from a deep well in the hypocentral zone of (A) the 1966 Tashkent earthquake ($M = 5.3$) and (B) an aftershock at Tashkent, $M = 4$. Arrows denote the origin times of the shocks.

Characteristic Time of premonitory effects

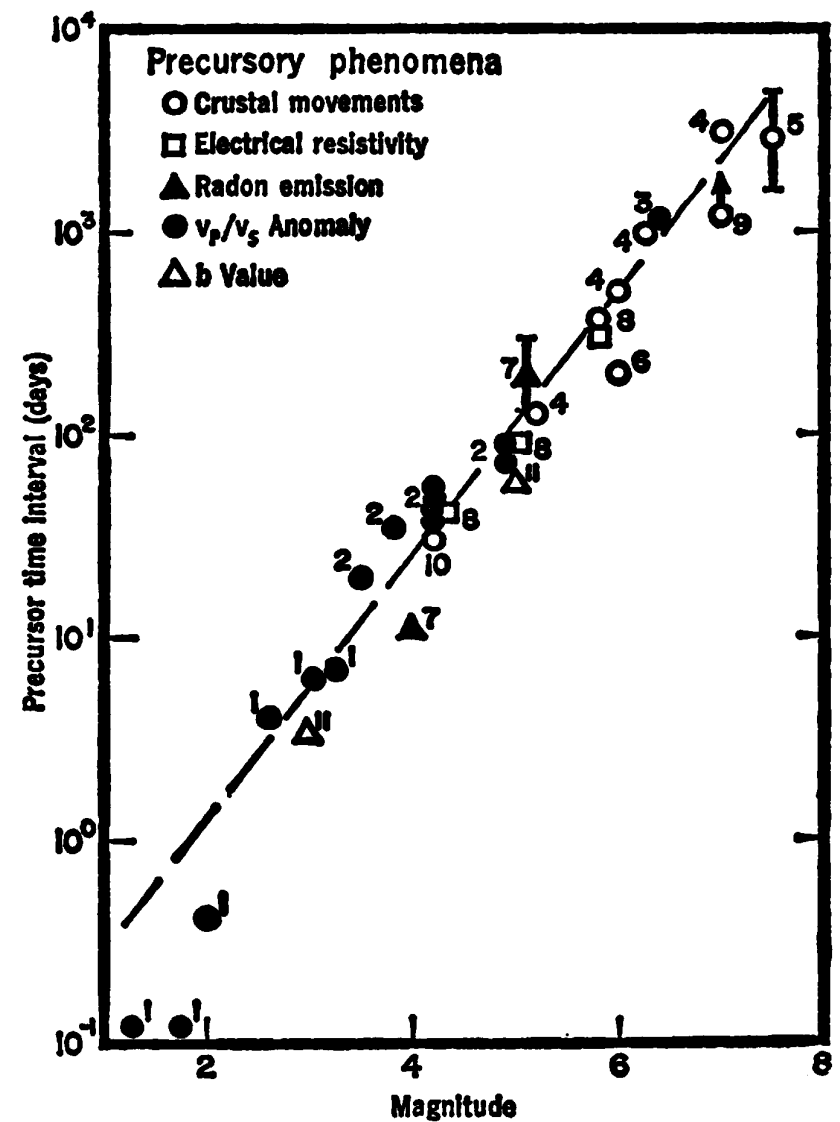


Fig. 8 (right). Duration time of various precursory phenomena as a function of earthquake magnitude. Earthquake location and data sources are as follows: point 1, Blue Mountain Lake, New York (2); point 2, Garm, U.S.S.R. (1); point 3, San Fernando, California (3); point 4, Kitamino, Kita-Izu, and Omi, Japan (24); point 5, Niigata, Japan (13); point 6, Odaigahara, Japan (15); point 7, Tashkent, U.S.S.R. (17); point 8, Garm, U.S.S.R. (10); point 9, Alma Ata, U.S.S.R. (25); point 10, Danville, California (16); and point 11, Fairbanks, Alaska (19).

Characteristic Time of premonitory effects

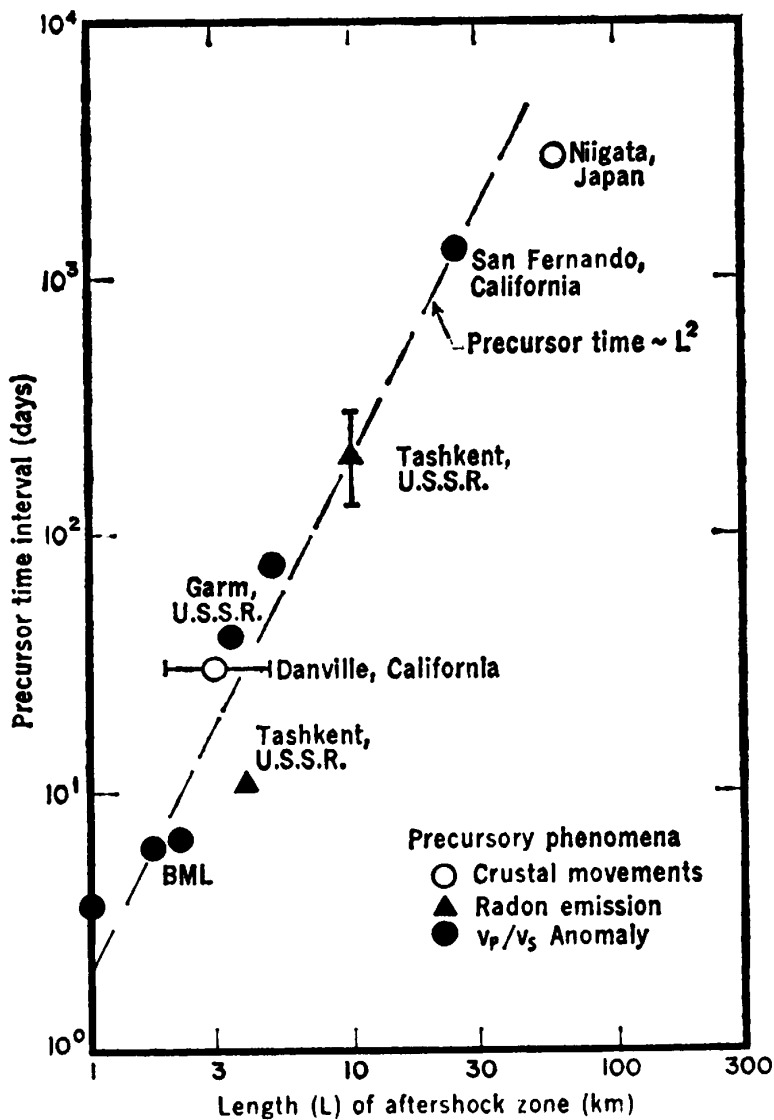


Fig. 9. Precursor time interval as a function of the length of the aftershock zone for a variety of earthquakes and types of physical observations. Note that a precursor time proportional to L^2 supports the model of the diffusion of fluids in the dilated zone. Data sources are the same as those in Fig. 8.